

Hole-Burning Spectroscopy and Relaxation Dynamics of Amorphous Solids at Low Temperatures

R. JANKOWIAK AND G. J. SMALL

The magnitude and temperature dependence of most of the properties of amorphous solids are anomalous at very low temperatures (≈ 1 Kelvin). Phonon-assisted tunneling of a distribution of glassy bistable configurations, or two-level systems, can account for these anomalies. A unified understanding of the low-temperature properties is required for an understanding of the glassy state. Persistent nonphotochemical hole burning of impurity optical transitions allows a glass state to be produced that is thermally inaccessible to the preburn state, and that allows the probing of tunneling dynamics on time scales that range between picoseconds and days. These data combined with recently obtained distribution functions for the two-level systems offer new insights into the tunneling dynamics.

IN THE EARLY 1970S TWO IMPORTANT DEVELOPMENTS OCCURRED that at the time seemed unrelated. One was the observation by Zeller and Pohl (1) of anomalous functional dependence with temperature of the specific heat and thermal conductivity of glasses at very low temperatures (≈ 1 K) and its theoretical interpretation as put forth by Anderson and co-workers (2) and Phillips (3). Their model was based on tunneling of glassy bistable configurations, which are often referred to as two-level systems (TLS). The intrinsic disorder of glasses provides a distribution of TLS or very low energy excitations that is unavailable to crystals. The notion of tunneling between points in the glass configuration space might conjure up the image of "life that exists in the cold." The second was the development with lasers of energy-selective spectroscopies in which two electronic sites are excited. Fluorescence line narrowing (FLN) emerged from the work of Szabo (4) and Personov and co-workers (5) on inorganic and organic doped solids, respectively. Persistent (in contrast with transient) hole burning was first observed by Kharlamov and co-workers (6) and Gorokhovskii and co-workers (7) for molecular systems. One can think of these spectroscopies as methods by which a narrow line laser "tricks" a disordered solid into mimicking one that is perfectly ordered. In principle this can result in the elimination of the site-inhomogeneous line-broadening contribution Γ_1 to the optical transition line width. Thus one has a frequency domain pathway to dynamics through the relation $T_2 = (\pi\Delta\nu_h)^{-1}$, where T_2 is the total dephasing time and $\Delta\nu_h$ is the homogeneous line width. The importance of this interplay between spectroscopy and dynamics was already apparent in the 1960s to "laserless" high-resolution spectroscopists who focused their attention on neat and doped

crystals. This focus is understandable since $\Gamma_1 \sim 2 \text{ cm}^{-1}$ for crystals, whereas in glasses Γ_1 is about two orders of magnitude greater. The crystal studies yielded valuable insights about a variety of phenomena, such as the optical dephasing from electron-phonon coupling, but the testing of theories was often limited by Γ_1 .

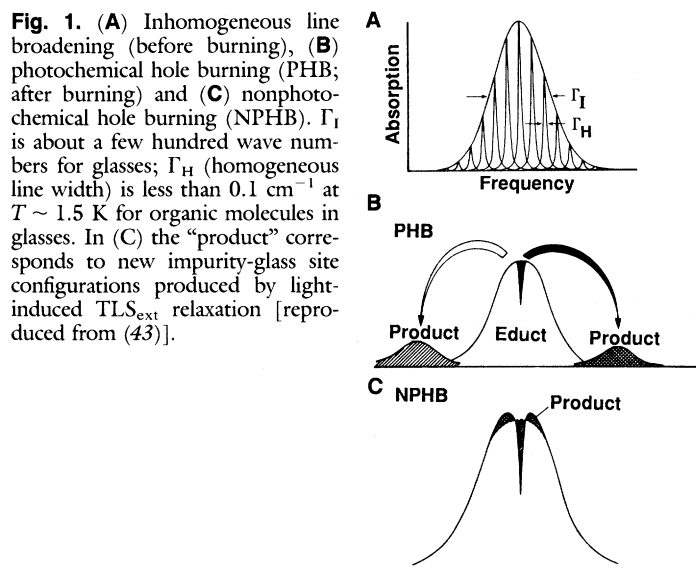
In the middle to late 1970s a connection was made between the dynamics of optical transitions of impurities in inorganic and organic amorphous hosts and phonon-assisted tunneling of the TLS (8–10). During the same period such tunneling was invoked to explain the phenomenon of nonphotochemical hole burning (NPHB). This type of hole burning and a second type, photochemical hole burning (PHB), are discussed below. For the moment one need only appreciate that FLN results in sharp fluorescence bands, whereas hole burning produces narrow holes or "windows" in an inhomogeneously broadened absorption profile. The holes are a manifestation of site-excitation energy-selective photobleaching. It is the mechanism for photobleaching that distinguishes NPHB and PHB.

Novel applications of line-narrowing spectroscopies abound. For example, one can generate high-resolution electronic spectra for biomolecules. Hole burning has potential for application to optical memory storage and to narrow highly transmitting optical filters. In recent years, however, much attention has been given to the use of hole burning to better understand dynamical processes in amorphous solids at low temperatures (11). In this article we discuss the different types of spectroscopic and dynamical data available from hole burning and explore how these data provide a window on the low-temperature dynamics that is distinct from, but complementary to, that afforded by other techniques (12).

Persistent Spectral Hole Burning

An absorption profile of an impurity (guest) electronic absorption transition that is site inhomogeneously broadened is depicted in Fig. 1A. The absorption profile is composed of individual homogeneously broadened site components that are unresolved. For amorphous hosts Γ_1 is large ($\sim 500 \text{ cm}^{-1}$). Uniform excitation of all sites would result in an equally broad and disappointing fluorescence spectrum. However, excitation (selection) of a narrow isochromat with a narrow-frequency light source (such as a laser) can result in a markedly narrowed fluorescence spectrum at low temperature, provided certain conditions are met (13). For example, the impurity concentration must be sufficiently low to preclude site randomiza-

R. Jankowiak is at the Ames Laboratory, Department of Energy, Ames, IA 50011. G. J. Small is at the Ames Laboratory, Department of Energy and Department of Chemistry, Iowa State University, Ames, IA 50011.



tion due to intermolecular energy transfer on a time scale comparable to the excited state lifetime. In addition, the fluorescence observed must originate from the electronic state being excited, which is a consequence of the fact that site energy distribution functions for different electronic states are generally not correlated.

With the notion of isochromat selection established by FLN, PHB followed logically. If the species that gives rise to the absorption is photoreactive, isochromat selective photobleaching can be engineered (Fig. 1B). In the first few years after 1974, PHB studies used crystalline hosts with impurities such as H_2 -phthalocyanine, free base porphyrin, and color centers. For the first two impurities, proton tautomerization is the photochemical mechanism, whereas photooxidation is operative for the latter. Hole widths as narrow as ~ 100 MHz were observed at 1.5 K.

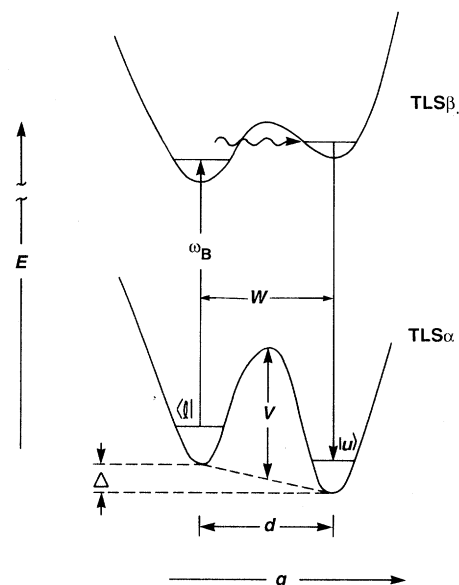
Photoreactivity of the absorbing species is not required in NPHB. What is required is a host with a “faulty memory” for its pre-excitation configuration near the absorber. That is, upon completion of the cycle from ground state to excited state and back to ground state, the host configuration must have changed more or less permanently if persistent holes are to be produced (Fig. 1C). With perhaps one or two exceptions, NPHB has only been observed with glasses and polymers (11, 14). Given the immense disorder (15) that exists in such hosts, this restriction is perhaps now not so surprising. However, at the time of the first observation of NPHB the low-temperature “gymnastic” abilities of glasses were not known to optical spectroscopists and thus its observation came as a pleasant surprise. In Fig. 2 the simple TLS model for the NPHB mechanism, as advanced in 1978 (16), is shown. It is consistent with the one mentioned earlier but includes some additional features. Thus it also approximates the bistable configurations of the glass with a distribution of asymmetric intermolecular double-well potentials (which are TLS). One has a distribution of barrier heights V , asymmetries Δ , and displacements d and may also have distinctly different intermolecular coordinates q . If we consider Fig. 2 a mechanism for persistent NPHB at $T = T_B$ (burn temperature) becomes apparent if we postulate that a subset of the distribution of TLS that interact with the impurity has the following properties at T_B ; namely, that relaxation between the two minima for the ground state is slow on the time scale of the experiment while, with the impurity excited, it is competitive with the excited state decay. The degree of competitiveness determines the hole-burning quantum efficiency. For example, with the burn frequency ω_B tuned to the “left” optical transi-

tion, barrier hopping or tunneling to the upper state leads to population of the right-well configuration in the ground state. It is the electron-TLS coupling that alters the TLS parameters such as V upon optical excitation. Figure 2 may well be an oversimplification since the optical excitation could conceivably trigger a chain of bistable configurational relaxation processes. Motion down a tendril (15) that links a series of potential energy minima could result in a final configuration around the ground state impurity that has almost the same optical excitation energy as the original preburn ground state configuration but that is kinetically inaccessible to it. Perhaps the most general definition of NPHB is that it stems from isochromat selective photobleaching, which is a manifestation of the production of a glass state that is thermally inaccessible at T_B to the original state.

One may ask whether the TLSs responsible for the initiation of hole burning have anything to do with the intrinsic TLSs (TLS_{int}) of the host. As discussed below, the former are distinct from those that cause optical dephasing and there are reasons to suggest that they are strongly associated with the impurity. Thus they shall be viewed here as extrinsic TLSs (TLS_{ext}).

At least at the lowest temperatures that have been used, NPHB is the result of phonon-assisted tunneling of TLSs and provides a most tangible illustration of TLS relaxation. Since 1983 NPHB has been shown to be a common phenomenon that can be observed for rare-earth ions in inorganic glasses and hydroxylated polymers, laser and organic dyes in the same polymers (for example, polyvinyl alcohol and polyacrylic acid) or alcohol glasses, aromatic molecules in polyacene amorphous films, self-aggregated dimers of chlorophyll in polystyrene, and the antenna protein complex of photosynthetic units. Although amorphous hosts with hydrogen-bonding capability often provide facile NPHB, the identification of highly efficient systems still occurs more by chance than by design. Figures 3 and 4 show recent examples for oxazine 720 in a glycerol glass and cresyl violet in a polyvinyl alcohol film. The quantum efficiency for the former is high (see below) and Fig. 3 shows that a series of sharp zero-phonon holes can be burned over the 30-GHz free spectral range of the single-frequency dye laser used for burning and reading (by transmission) of the spectrum. The zero-phonon holes are not accompanied by phonon side-band holes (discussed below), which indicates very weak linear electron-phonon coupling. Figure 4 illustrates that detailed vibronic data for impurity molecules can be obtained. Although hole burning is observable for a wide range of

Fig. 2. The two-level system (TLS) model for nonphotochemical hole burning, where $\langle l \rangle$ and $\langle u \rangle$ are the lower and upper states. The subscripts α and β label the TLS that interact with the impurity in its ground and excited electronic states. The tunnel frequency W depends on the tunnel parameter λ as $\hbar\omega_0 e^{-\lambda}$; λ is defined as $d(2mV)^{1/2}/\hbar$, where m is the tunneling mass. The frequency ω_B is that of the burn laser. See text for further discussion and definitions.



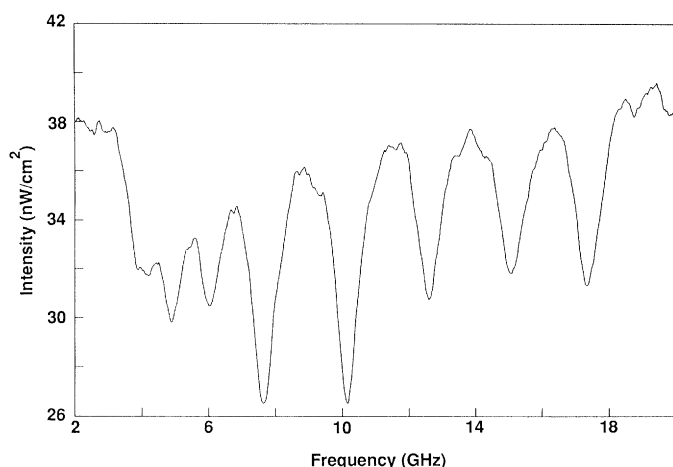


Fig. 3. Series of nonphotochemical holes for the laser dye oxazine 720 embedded in a glycerol glass at $T_B = 1.4$ K. The widths for the five most intense holes are ~ 0.33 cm^{-1} (absorption intensity decreases from top to bottom). The burn wavelengths are near 6490 Å, the burn intensity is 40 nW/cm^2 , and the burn time is 60 seconds.

burn frequencies, the spectrum shown was obtained for ω_B on the high-energy side of the absorption profile. The upper curve is the preburn absorption. If we consider for now only the middle spectrum, in addition to the hole at ω_{B_1} vibronic “satellite” holes are observed and are most pronounced at frequencies below ω_{B_1} . The displacements between these holes and ω_{B_1} are the excited state frequencies of the Franck-Condon allowed impurity vibrational modes. For example, the hole at 527 cm^{-1} is due to sites whose origin (zero-phonon) transition lies at $\omega_{B_1} - 527$ cm^{-1} . They absorb ω_{B_1} radiation through their vibronic transition at 527 cm^{-1} . Subsequent to this absorption, intramolecular vibrational relaxation occurs to the zero-point level, after which hole burning ensues.

Satellite holes associated with the lower frequency (≤ 100 cm^{-1}) modes of the system can also be produced. They are referred to as phonon side-band holes. An example is shown in Fig. 4B at a frequency 32 cm^{-1} less than that of ω_{B_1} . The phonon side-band hole is often broad due to frequency-dependent coupling to a distribution of phonons. The phonon side band (and zero-phonon hole) can be used to characterize the linear electron-phonon coupling.

Types of Dynamical Data

With NPHB one can study dynamical relaxation processes in glasses whose time scales vary over about 15 orders of magnitude (picoseconds to hours). This versatility results from the following types of measurements: optical dephasing and spectral diffusion (from the zero-phonon hole width), hole-growth kinetics, spontaneous hole filling, thermal annealing and cycling, and laser-induced hole filling. We will consider only the first three in detail and then assess the extent of our understanding of the structures of TLSs in amorphous solids.

Laser-induced hole filling is the filling (or erasure) of a primary hole burned at ω_{B_1} at $T = T_{B_1}$, which results from subsequent irradiations at ω_{B_2} ($T_{B_2} = T_{B_1}$) within the inhomogeneously broadened absorption profile (17) (Fig. 4C). It is not a bulk heating effect due to absorption at ω_{B_2} . The mechanism does not appear to involve antihole site excitation followed by reversion back to preburn (ω_{B_1}) configurations. Rather, irradiation (absorption) at ω_{B_2} of sites that are not connected with those burned at ω_{B_1} appears to trigger glass configurational transitions that lead to global spectral diffusion (17). This spectral diffusion would lead to filling of the ω_{B_1} gradient in

excitation-frequency space. This mechanism is viable only if long-range communication or connectivity exists between spatially removed impurity sites. The kinetics of laser-induced hole filling have not yet been explored. The thermal cycle experiment involves the burning and reading of a hole at $T = T_B$ followed by reading at $T_R > T_B$ and finally again at T_B to complete the cycle. Not only can partial or complete (if T_R is sufficiently high) hole erasure occur, but hysteresis for the hole width is generally encountered. A simple model based on thermally induced spectral diffusion from TLS relaxation has been developed to explain the increase in hole width at T_B after the thermal cycle (18). These relaxation processes occur with the impurity in its ground electronic state (that is, in the dark), as is the case for spontaneous hole filling (see below).

The Optical Hole Shape and Hole-Growth Kinetics

The development of an expression for the zero-phonon hole profile (coincident with ω_B) is reasonably straightforward (19). One defines $N_0(\omega - \omega_m)/N$ as the probability of finding a site with a zero-phonon transition frequency equal to ω , a Gaussian distribution for the site-excitation distribution function N_0 is usually used. The quantities N and ω_m define the total number of sites and the most probable transition frequency, respectively. The absorption cross section, burn-laser photon flux, and hole-burning quantum

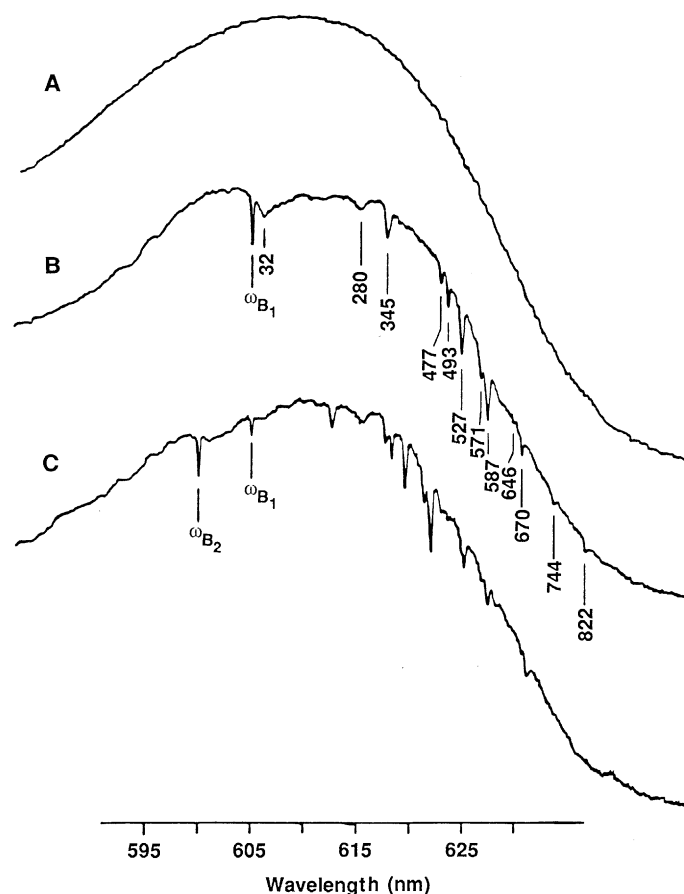


Fig. 4. Nonphotochemical hole burning for the laser dye cresyl violet in polyvinyl alcohol film at $T_B = 1.8$ K. (A) Preburn absorption; (B) hole-burned spectrum obtained with ω_{B_1} ; and (C) hole-burned spectrum obtained with ω_{B_2} after the burn at ω_{B_1} . The burn at ω_{B_2} has significantly filled (erased) the ω_{B_1} -produced spectrum. This is an example of the laser-induced hole filling discussed in the text.

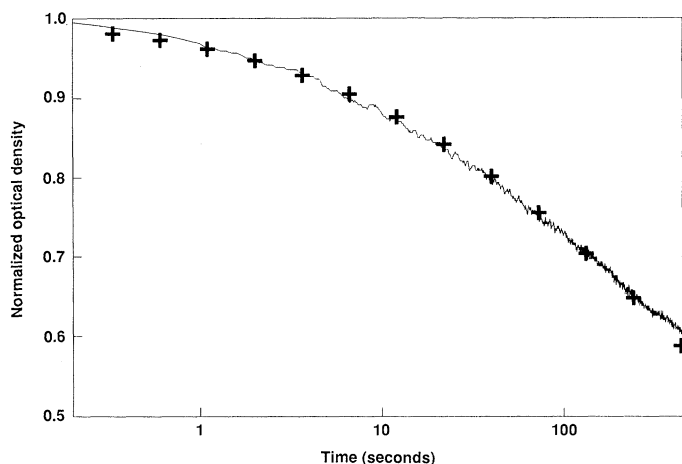


Fig. 5. Hole-growth kinetics for oxazine 720 in a glycerol glass at $T_B = 1.4$ K. The solid curve is experimental and obtained with a photon flux $P \approx 0.82 \times 10^{11} \text{ cm}^{-2} \text{ sec}^{-1}$ (25 nW/cm² at 6490 Å); the (+) represents the theoretical fit to the dispersive kinetics calculated with $\sigma = 0.27 \times 10^{-12} \text{ cm}^2$ (see text and Table 1).

yield are defined as σ , P , and ϕ , respectively. After a burn for time τ at a frequency of ω_B , the number of absorbers that remain at the excitation frequency ω is given by

$$N_\tau(\omega - \omega_m) = N_0(\omega - \omega_m) \exp[-\sigma P \phi \tau \ell(\omega_B - \omega)] \quad (1)$$

The function ℓ is the homogeneous Lorentzian line shape for the single-site absorption transition. For several reasons it is advantageous to work in the short-burn time limit such that $\exp(-x) \sim 1 - x$. Then the hole profile is given by

$$A_0(\Omega) - A_\tau(\Omega) = \sigma P \phi \tau \int d\omega N_0(\omega - \omega_m) \ell(\omega_B - \omega) \ell(\Omega - \omega) \quad (2)$$

where $A_0(\Omega)$ and $A_\tau(\Omega)$ are the pre- and afterburn absorption intensities at frequency Ω . For the frequently encountered situation where Γ_1 of N_0 is much greater than $2T_2^{-1}$ ($\Delta\nu_h$ is thus the full width at half-maximum of ℓ), N_0 may be removed from the integral. Thus the hole profile is the convolution of two Lorentzians that yields a Lorentzian hole profile centered at $\Omega = \omega_B$ with a full width defined as $\Gamma_{\text{hole}} = 2\Delta\nu_h$.

One can question the validity of Eq. 1 for NPHB in amorphous solids since there should be a distribution of quantum yield values ϕ that stems from disorder. The kinetics for hole growth would then be dispersive. Figure 5 shows one example of these phenomena for oxazine 720 in a glycerol glass. A knowledge of the TLS distribution function is required to interpret the dispersive kinetics associated with TLS tunneling and the temperature-dependent properties such as specific heat, thermal conductivity, and optical dephasing. A consideration of TLS_{int} or TLS_{ext} or both may be necessary. Prior to 1986, a substantial number of phenomenological distribution functions appeared (11) that mainly considered the TLS_{int} . The notion of “uniformity” for the distribution was first introduced and led to a constant density of states function [DOS, $\rho(E)$]. In this case $E^2 = \Delta^2 + W^2$, where E is the tunnel state splitting, and W is the tunneling frequency given by $W = \hbar\omega_0 \exp(-\lambda)$ (Fig. 2) [\hbar is Planck’s constant and λ is the tunnel parameter given by $\lambda = d(2mV)^{1/2}/\hbar$, where m is the mass of the tunneling entity (Fig. 2)]. The normalized distribution function $P(\Delta, \lambda)$ equal to \bar{P} (a constant) for $\lambda_{\text{min}} \leq \lambda \leq \lambda_{\text{max}}$ and $\Delta_{\text{min}} \leq \Delta \leq \Delta_{\text{max}}$ ($P = 0$ otherwise) was proposed (2, 3). This model leads to $\rho = \rho_0$ (constant); initial experiments showed that the linear variation of the specific heat of inorganic glasses with T (for $T \leq 1$ K) could be explained.

Subsequently, phenomenological functions were introduced to account for specific heat and thermal conductivity data that indicated that $\rho(E)$ is a slowly increasing function of E . It is important to emphasize that the above distribution function can lead to a prediction for the dispersive kinetics associated with hole growth or spontaneous hole filling discussed below. The prediction was that the observable quantity should exhibit a logarithmic dependence on time (20, 21). Figure 5 represents only one of several cases where this prediction is not met over the entire time regime. Such data and questions related to the temperature dependence of optical dephasing have recently stimulated a derivation of analytic forms for the TLS distribution and DOS functions (22). Two assumptions are involved: (i) that Gaussian distribution functions (GDF) govern the distributions for Δ and λ (centered about $\Delta_0 \sim 0$ and λ_0 with variances σ_1 , and σ_2) and (ii) that the stochastic variables Δ and λ are independent. The GDFs for λ and $\tilde{\Delta}$ are $g(\lambda_0, \sigma_2^2)$ and $g(\tilde{\Delta}_0, \tilde{\sigma}_1^2)$, respectively, where the normalized asymmetry parameter $\tilde{\Delta} = \Delta/(\hbar\omega_0)$ and variance $\tilde{\sigma}_1^2 = \sigma_1^2/(\hbar\omega_0)^2$ are used. The function $\rho(E)$ obtained with these distribution functions will be discussed below in the context of optical dephasing.

Hole-growth kinetics have been successfully modeled in terms of a rate expression obtained from

$$\int_0^k dR f(R) \exp(-R't)$$

where $R' = P\sigma R/k$, $P\sigma$ is the induced absorption rate (23, 24), R is the TLS_{ext} relaxation frequency associated with NPHB, k^{-1} is the impurity excited state lifetime, and $f(R)$ is the distribution function for R . For sufficiently large dispersion in R (a situation often encountered) the above integral is well approximated by (24)

$$\int_{1/t}^{P\sigma} dR' f(R')$$

where $1/t$ is the minimum relaxation rate. From the TLS model one has $R \propto W^2$. Because $W^2 \propto \exp(-2\lambda)$ (Fig. 2) and because λ depends on several variables that are subject to statistical variations, the dispersion of R is determined primarily by W^2 . The function $f(R)$ is readily obtained from $g(\lambda_0, \sigma_2^2)$. Data of the type given in Fig.

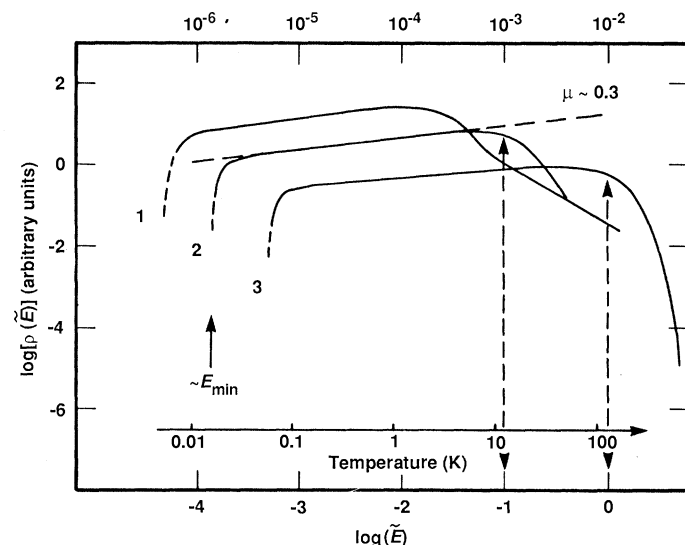


Fig. 6. Dependence of the TLS_{int} density of states on tunnel splitting E (also T and $\bar{E} = E/(\hbar\omega_0)$ for $\hbar\omega_0 = 10^{-2} \text{ eV}$). Curves are calculated with $\lambda_0 = 5$, $\sigma_2 = 3$, and $\Delta_0 = 0$ for three $\tilde{\sigma}_1$ values: curve 1, $\tilde{\sigma}_1 = 0.02$; curve 2, $\tilde{\sigma}_1 = 0.1$; and curve 3, $\tilde{\sigma}_1 = 1.0$. E_{min} marks the onset of the gap for curve 2. The central region of curve 2 has a slope $\mu \sim 0.3$.

Table 1. Dispersive hole-growth and spontaneous hole-filling kinetics for oxazine 720 in glycerol at $T = 1.4$ K. The value for $\langle\phi\rangle$ was calculated with $k = 3.7 \times 10^8 \text{ sec}^{-1}$; for the hole-growth kinetic analysis a value of $\sigma = 0.27 \times 10^{-12} \text{ cm}^2$ was used.

Process	λ_0	σ_2	$\langle R \rangle$	$\langle \phi \rangle$	$\langle \phi \rangle_{\zeta = 0.05}$
Hole growth	8.5	1.8	2.7×10^7	6.8×10^{-2}	0.59
Spontaneous hole filling	18	1.5	2.3×10^{-2}		

5 can be satisfactorily accounted for with this model. From the fit, the distribution parameters λ_0 and σ_2 are obtained and consequently the average value $\langle R \rangle$ is $[\Omega_0 \exp(-2\lambda_0)] \exp(2\sigma_2^2)$. The frequency Ω_0 is defined by $R = \Omega_0 \exp(-2\lambda)$. The dispersion provides an amplification for $\langle R \rangle$ over $R_0 = \Omega_0 \exp(-2\lambda_0)$, which is the relaxation frequency for a nondispersive system. Values for $\langle R \rangle$, λ_0 , σ_2 , and the average quantum yield $\langle \phi \rangle$, which is equal to $\langle R \rangle / (\langle R \rangle + k)$, are given in Table 1. The quantities $\langle R \rangle$, $\langle \phi \rangle$, and σ_2 are characteristic of the system but too much significance should not be attached to λ_0 since Ω_0 is arbitrary. To be consistent with earlier work we have used $\Omega_0 = 10^{12} \text{ sec}^{-1}$ (an estimate for the TLS zero-point frequency). Oxazine 720 in glycerol appears to have one of the highest $\langle R \rangle$ values for NPHB measured to date (Table 1). For simplicity, the inherent dispersion that arises from the random distribution of transition dipoles in the glass and the absorption line shape are not taken into account in the equations given above for the kinetics. When taken into account, the σ_2 value given in Table 1 is reduced by ~ 307 . Table 1 also includes an average quantum yield $\langle \phi \rangle_{\zeta}$ that corresponds to the initial fraction ζ ($\zeta = 0.05$) of the hole burning.

Spontaneous Hole Filling

Although nonphotochemical holes can persist for long periods of time (on the order of days), slow filling or erasure is generally observed with the sample in the dark and held at $T = T_B$. The relaxation processes responsible for spontaneous hole filling (SPHF) occur with the impurity in its ground electronic state. The average relaxation time $\langle R \rangle^{-1}$ associated with SPHF is several orders of magnitude longer than that for hole growth. Spontaneous hole-filling kinetics have been studied in several systems, such as oxazine 720 in glycerol. The use of the approach discussed above for hole growth leads to a rate expression for SPHF (23) that can account equally well for the kinetics. As for the underlying physics, two models have been proposed; one views SPHF as a manifestation of global spectral diffusion that results from “democratic” TLS relaxation processes (which includes those TLSs not connected with the burn); and the other attributes SPHF to antihole reversion that involves the TLS_{ext} involved in the burn. Under certain circumstances the latter can lead to filling without hole broadening.

We can write $\langle R \rangle = \Omega_0 \exp(-2\lambda_0) \exp(2\sigma_2^2)$ as the average relaxation frequency for SPHF. However, the distribution function parameter values will be different, since SPHF is a slower ground state process (Table 1). For $\Omega_0 = 10^{12} \text{ sec}^{-1}$, the data for oxazine 720 in glycerol lead to $(\lambda_0, \sigma_2) = (18, 1.5)$ for SPHF in contrast with $(8.5, 1.8)$ for hole growth.

It is significant that the “nonphenomenological” (but still simple) distribution functions that have been introduced can describe dispersive kinetics that result from TLS relaxation processes that occur on the time scales indicated in Table 1. These distributions can account for deviations from the logarithmic time dependence predicted by earlier TLS distribution functions. Also, the time regime

over which $\ln(t)$ behavior occurs can be defined. Below we explore the use of the distribution functions for understanding much faster optical-dephasing processes.

The Optical Line Width and Dephasing

Like specific heat and thermal conductivity, the optical line width (hole width) and pure optical-dephasing frequency $(T_2^*)^{-1}$ of impurity transitions are anomalous in glasses at very low temperatures (Table 2). The pure dephasing frequency $(T_2^*)^{-1}$ is related to the total dephasing frequency (T_2^{-1}) by the relation $T_2^{-1} = (2T_1)^{-1} + (T_2^*)^{-1}$, where T_1 is the depopulation decay time of the excited electronic state. Not only are the temperature dependences of properties in glasses distinctly different than in crystals (Table 2) but also their magnitudes are different. FLN measurements on rare-earth ions and NPHB measurements on aromatic molecules first demonstrated that the temperature dependence of the optical line width is markedly different in glasses than in crystals. Since 1980 a wide variety of systems have been studied and photon-echo techniques have now been used. For organic systems, the optical line width or T_2^{-1} or both typically follow a T^n power law with $1.0 \leq n \leq 1.5$ (Table 2). Most measurements have been confined to $T \leq 10$ K and many to $T \leq 4.2$ K. Many molecules, including free base porphyrins, have a hole-width dependence of $T^{1.3}$ for $T \leq 4.2$ K (25, 26). Several rare-earth ion transitions, for example, the ${}^4F_{3/2}(I)$ transition of Nd^{3+} in a pure SiO_2 glass, fit into the above range of n values, although others have been observed with $n \sim 2$. For the purposes of this article we explore how phonon-assisted tunneling of TLSs can account for the range of power laws given in Table 2.

Theories based on off-diagonal (ODM) and diagonal (DM) modulation of transitions due to the impurity-TLS interaction have been developed. The interaction is described by

$$H_{12} = \sum_{\rho=\alpha,\beta} \left[\frac{V_{\rho}\Delta}{E} \{ |\psi_1\rangle\langle\psi_1| - |\psi_2\rangle\langle\psi_2| \} + \frac{V_{\rho}W}{E} \{ |\psi_1\rangle\langle\psi_2| + |\psi_2\rangle\langle\psi_1| \} \right] |\rho\rangle\langle\rho| \quad (3)$$

where H_{12} is the Hamiltonian, $|\psi_1\rangle$ and $|\psi_2\rangle$ are the tunnel states, and α and β are the labels for the ground and excited state impurity states. The term $V_{\rho} = \frac{1}{2}(V_{\ell\rho} - V_{u\rho})$ represents the difference in the

Table 2. Properties of glasses and crystals at very low temperatures. The experimental power laws for the specific heat and thermal conductivity were determined for $T \leq 1$ K. For the TLS model with averaging, the TLS_{int} were obtained with λ_0 from about 5 to 7 and σ_2 from about 3 to 5. For the TLS_{ext} λ_0 was about 12 to 16 and σ_2 was about 1.5 to 3.

Property	Crystal	Glass		
		Ex-periment	Standard TLS model	TLS model with averaging
Density of states*	E^2, DP		$\rho_0 = c$	E^{μ}
Optical line width, dephasing time†	T^7	T^{n_1}	T^2 (DM) T^2 (ODM)	T^{n_2}
Specific heat‡	T^3	T^{n_3}	T	T^{n_4}
Thermal conductivity§	T^3	T^{n_5}	T^2	T^{n_6}

*For the TLS_{int} , $0.1 \leq \mu \leq 0.5$, whereas $\mu \sim 0$ for TLS_{ext} ; DP, Debye phonons; c is a constant. † $1.0 \leq n_1 \leq 1.5$; for the TLS_{int} in the DM model, $1.2 \leq n_2 \leq 1.5$. ‡ $1.0 \leq n_3 \leq 1.5$; for the TLS_{int} , $1.2 \leq n_4 \leq 1.5$. § $1.8 \leq n_5 \leq 2.0$; for the TLS_{int} , $1.8 \leq n_6 \leq 2.0$.

interaction between the impurity and the lower (ℓ) and upper (u) localized oscillator states of the TLS. The first and second terms of Eq. 3 are the diagonal and off-diagonal modulations. The TLS-phonon interaction (not in Eq. 3) is needed to allow for absorptive and emissive transitions between the tunnel states. A difficulty for the ODM and DM theories or, more generally, theories that pertain to the low-temperature behavior of any property has been the question of how to perform the configurational averaging over the TLS. To illustrate the magnitude of the problem, consider the phonon-assisted relaxation frequency for a single TLS τ^{-1} , given as

$$\tau^{-1} = K W^2 f^2 E \operatorname{ctnh}[E/(2k_B T)] \quad (4)$$

Here f is related to the deformation potential, which measures the difference in coupling of the left and right wells of the TLS to the phonon bath, K is a collection of constants, and k_B is Boltzmann's constant. That f and $W(E)$ are uncorrelated appears to be a reasonable assertion. However, it has often been assumed without rigorous justification that $\langle W^2 \rangle = E^2$. With this assumption $\langle \tau^{-1} \rangle$ is readily obtained by multiplying Eq. 4 by $\rho(E) \sim E^\mu$ and integrating between 0 and E_{\max} (the maximum tunnel splitting or phonon frequency, whichever is greater). In the low-temperature limit ($k_B T \ll E_{\max}$), for example, $\langle \tau^{-1} \rangle \propto T^{4+\mu}$. However, without knowledge of the TLS distribution function one does not know what value of μ is consistent with $\langle W^2 \rangle = E^2$ (or whether this equality is valid). Often the value of μ is simply chosen to achieve agreement with experiment. This approach can be avoided by using the TLS distribution functions discussed earlier. These distribution functions have been used to derive analytic expressions for τ^{-1} , $\rho(E)$, and the dephasing frequencies due to ODM and DM (22, 27).

The DM theory for the optical line width or pure dephasing frequency $(T_2^*)^{-1}$ appears to be most consistent with experiment. Recent photon-echo studies have shown that the decays on the picosecond time scale can be remarkably nondispersive (28), in contrast with the kinetics for NPHB and SPHF. In the DM theory, dephasing occurs through the interaction of the impurity with a "sea" of weakly interacting TLS_{int} . For a large enough sea, each and

every impurity should undergo phase-memory loss with the same characteristic time constant. In contrast, dephasing from ODM would result from a relatively strong interaction with one or a small number of nearby TLSs (perhaps a TLS_{ext}). This strong interaction should be subject to significant dispersion (witness the large Γ_1 in glasses) and thus dephasing due to ODM could be expected to be dispersive. The DM theory (29) predicts that the optical line width $\langle \langle \Delta\omega \rangle \rangle$ is given by (21)

$$\langle \langle \Delta\omega \rangle \rangle = \langle \langle \operatorname{sech}^2[E/(2k_B T)] \tau^{-1} \rangle \rangle \quad (5)$$

with τ^{-1} defined by Eq. 4. Equation 5 pertains to the slow-modulation limit where $V' = |V_\beta - V_\alpha| \Delta/E > \tau^{-1}$ (that is, motional narrowing does not occur, in agreement with experiment). But also it is assumed that $V' < E$ (weak coupling). The averaging in Eq. 5 is done by first summing over all TLSs of a given E under the constraint $V' > \tau^{-1}$; the averaging is then performed over the parameters Δ and W . The first averaging (spatial integration) assumes a cutoff radius r_c for each E that is determined by $\tau^{-1} = b\Delta/(r_c^s E)$, where b and s are constants. A multipolar impurity-TLS interaction given by br^{-s} is used. With $s = 3$ (dipole-dipole interaction) it is possible to account for a dephasing power law of T^n with $1 \leq n \leq 1.5$. With the above distribution functions, $\langle \tau^{-1} \rangle_{\bar{E}}$ and $\langle \Delta \rangle_{\bar{E}}$ can be obtained and used to show that in the low temperature limit $\langle \langle \Delta\omega \rangle \rangle \propto T^{1+\nu}$ ($s = 3$). Thus with $\nu \sim 0.3$, the power law that is observed for many systems is attained. Such a value emerges from the theory for $\lambda_0 \sim 5$ and $\sigma_2 \sim 3$. Notice the marked difference between these values and those obtained for hole growth and for SPHF (Table 1). A key question is what value of μ in the DOS $\rho(E) \sim E^\mu$ arises with $\lambda_0 \sim 5$ and $\sigma_2 \sim 3$? The answer is $\mu \sim 0.3$. Variations of μ by ± 0.2 are attained when λ_0 and σ_2 are allowed to vary in the ranges 5 to 7 and 3 to 4, respectively. This indicates that the value of μ is very sensitive to the ratio of λ/σ_2^2 . For λ_0 as large as ~ 12 , $\mu \sim 0$ (with the distribution function for Δ still centered near or at zero) and $\nu \sim 2$. Is there a connection between the dephasing and, for example, specific heat? It seems that there may be since the same range of λ_0 and σ_2 values that account for the temperature dependence of dephasing with the DM theory are consistent with the observed power laws in temperature for specific heat. Much evidence suggests that the TLS_{int} is a major contributor to the specific heat for $T \lesssim 1$ K. Thus the implication of TLS_{int} for dephasing due to DM seems reasonable. The TLSs responsible for dephasing are distinctly different from those responsible for hole formation and SPHF. The "faster relaxing" TLSs associated with dephasing do not contribute to persistent hole formation since their tunnel states are effectively in thermal equilibrium (with the impurity in its ground state). Conversely, the "slower relaxing" TLS_{ext} responsible for hole growth do not contribute to the dephasing or homogeneous line width (consistent with the low quantum yields for NPHB).

Very recently, the distribution functions $g(\lambda_0, \sigma_2^2)$ and $g(\Delta_0, \sigma_1^2)$ have been used with the Monte Carlo simulation (MCS) technique to determine $\rho(E)$ over the entire range of tunnel state splittings (30). Some of the results which pertain to the TLS_{int} are shown in Fig. 6 for $(\lambda_0, \sigma_2) = (5, 3)$, $\hbar\omega_0 = 10^{-2}$ eV, and three values of $\bar{\sigma}_1 = \sigma_1/(\hbar\omega_0)$. For the central region of curves 1 through 3, in which $\rho(E) \propto E^\mu$, the value of μ is determined principally by the values of λ_0 and σ_2 as predicted earlier (22). The crossover at a higher $\bar{E} = E/(\hbar\omega_0)$ value to a negative slope for $\rho(\bar{E})$ occurs at $\bar{E} \sim \bar{\sigma}_1$. The distribution functions yield a gap in the DOS which has an onset at a very low tunnel state splitting (E_{\min}). The value of E_{\min} depends on λ_0 , σ_2 , and $\bar{\sigma}_1$, but the gap has its origin in the distribution function for the tunneling frequency W . Curve 2 of Fig. 6 for $\bar{\sigma}_1 = 0.1$ is characterized in part by $\mu \sim 0.3$ for the central region of the DOS. Vitreous silica exhibits a temperature power law

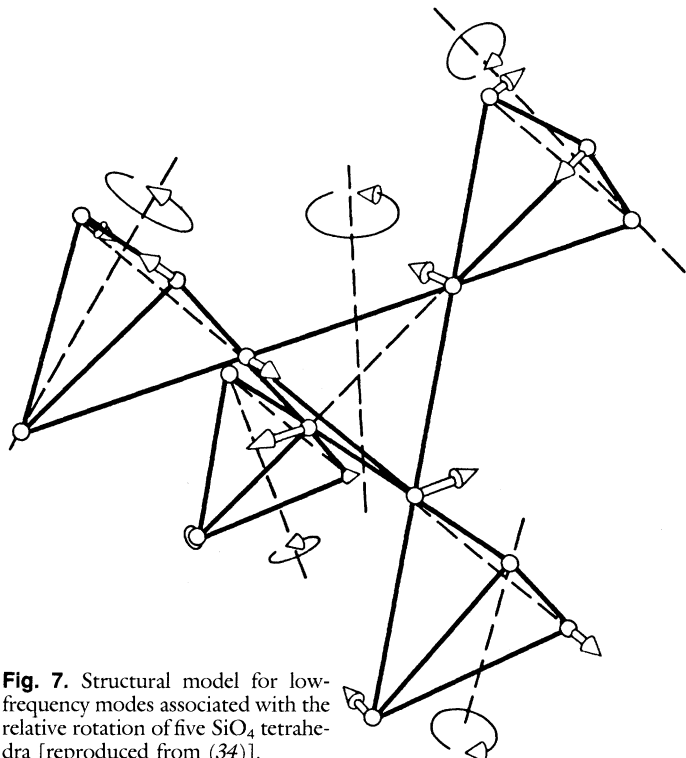


Fig. 7. Structural model for low-frequency modes associated with the relative rotation of five SiO_4 tetrahedra [reproduced from (34)].

for specific heat of $T^{1+\mu}$ with $\mu = 0.35 \pm 0.05$ for $0.03 \leq T \leq 1$ K (31, 32). Moreover, this work led to a value of 15 mK for E_{\min} . The onset of the gap for curve 2 is in reasonable agreement with this value. Taken together, the exponent μ and E_{\min} provide a quite stringent test for TLS distribution functions. The good agreement between the results of Lasjaunias and co-workers (31, 32) for vitreous silica and those of Fig. 4 suggests that the assumptions which underlie our model are reasonable.

Nature of the TLS?

Little progress on determining the actual nature of the TLS has been made. Even for amorphous silicon dioxide, the most widely studied material, there is no microscopic description that has generally been agreed upon, although recent calculations (33, 34) suggest that hindered rotations of several connected SiO_4 tetrahedra are reasonable candidates for the TLS excitations (or at least a fraction thereof). The structural model of Buchenau and co-workers (34) for the low-frequency excitations associated with the concerted hindered rotation of five tetrahedra is shown in Fig. 7. The TLS asymmetric double-well potential associated with this motion exhibits a Δ of about 2 cm^{-1} and a barrier height of several wave numbers (33). The width of the Δ -distribution that corresponds to curve 2 of Fig. 4 is about 18 cm^{-1} , which is about the correct order of magnitude.

The basic structural units of amorphous water prepared at low temperature are H_2O tetrahedrons. Recently, Härdle and co-workers (35) have discussed the nature of tunneling in this system. Although protons might seem to be predestined to be the tunneling entities, the studies of elastic properties showed that there is no isotopic effect associated with deuteration (35). This suggests a connection with vitreous silica in that, for amorphous water, the tunnel states may be associated with relatively large (hydrogen-bonded) networks. Concomitantly, large-amplitude proton motions would not be associated with the tunneling coordinate.

What then can be said for the molecular systems on which this article has focused? If we consider the hydroxylated polymers and alcohol glasses that can hydrogen bond, then there are data that address the question. Recent studies on tetracene in an ethanol-methanol glass (36), oxazine 720 in polyvinyl alcohol (37), resorufin in glycerol (38), and quinizarin in an ethanol-methanol glass (39) have shown that the hole-growth kinetics are markedly slowed (couple orders of magnitude) by deuteration of the hydroxyl group. In sharp contrast, the magnitude and temperature dependence of the hole width and dephasing are unaffected. These findings are consistent with the previously discussed model that invokes two “types” of TLS, TLS_{int} and TLS_{ext} . The latter, which are responsible for hole growth, have tunnel coordinates that involve considerable amplitude for the hydroxyl proton; however, the coordinates for the TLS_{int} , which are responsible for dephasing, do not. This in turn suggests that the TLS_{int} are far more spatially extended than the TLS_{ext} . For polymers subtle and hindered cooperative motion of chains may be associated with the TLS_{int} . For the alcohol glasses, extended hydrogen-bonding networks may be the key to understanding the TLS_{int} as may also be the case for amorphous water.

Concluding Remarks

Although our understanding of the structural and dynamical aspects of tunneling between points in the configuration space of the glass is far from complete, hole burning is a useful and multifaceted approach for studying tunneling phenomena. The data span an

impressive dynamical time range and have been instrumental for the development of “nonphenomenological” TLS distribution functions. These functions allow for comparison of the dispersions that are associated with different properties of the same system and a systematic comparison of properties between different systems. It seems particularly important that many if not all of the available experimental techniques be brought to bear on a single system. In addition to NPHB, these include photon echo, specific heat (including time-dependent measurements), thermal conductivity, ultrasonic absorption, and neutron scattering measurements.

In the discussion of the pure optical dephasing time T_2^* due to TLS_{int} tunneling, the question of whether the hole width does generally provide a reliable route to T_2^* was not raised. Recent photon-echo and NPHB studies of resorufin in an ethanol glass by Fayer and co-workers (28) suggest, as had earlier time-dependent hole-burning studies (40), that this may not be the case even when low burn intensities ($\approx 1 \mu\text{W}/\text{cm}^2$) and shallow (few percent occupation) holes are used. Under these conditions, the fact that the hole width is greater than $2(\pi T_2)^{-1}$ may be because the hole burning and reading forms a relatively long experiment (several seconds). Thus slow TLS relaxation processes (relative to the population decay time T_1) may lead to spectral diffusion or hole broadening (39). There is evidence that hole filling can occur during the burn; this filling may be related to the laser-induced hole-filling phenomenon. Thus the understanding of the “additional” hole broadening may shed light on the long-range communication between impurity sites that may occur only in amorphous solids. Perhaps connectivity between different TLS could be used to model this communication.

We have not yet mentioned that there appears to be a consistent discrepancy between the temperature power laws ($T \leq 1$ K) for specific heat and thermal conductivity when the $\rho(E) \propto E^\mu$ power law is used for interpretation (41). For the static experiments, our preliminary calculations with the distribution functions in this article indicate that the discrepancy can be removed provided that the specific heat is governed by tunneling of both a TLS_{int} and a TLS_{ext} distribution. The thermal conductivity is determined by only the faster relaxing TLS_{int} distribution. The time-dependent specific heat data for vitreous silica (42) also indicate that tunneling by TLS_{ext} is important at longer times.

The two problems mentioned above demonstrate the importance of time-dependent techniques that are capable of measuring the magnitude and temperature dependence of properties in glasses over different time windows. The data for each window would establish parameters for those bistable configurations that contribute to relaxation within the window. The “effective” TLS density of states, for example, would depend on the time interval and this dependence would provide a stringent test for TLS distribution functions and the TLS model itself.

Finally, an expanded effort on theoretical modeling of the structures associated with the TLS_{int} is desirable. As discussed above, the TLS_{int} of organic and inorganic systems may be similar in that they involve spatially extended networks and cooperative tunneling motion in which the displacement for any atom is very small.

REFERENCES AND NOTES

1. R. C. Zeller and R. O. Pohl, *Phys. Rev. B* **4**, 2029 (1971).
2. P. W. Anderson, B. I. Halperin, C. M. Varma, *Philos. Mag.* **25**, 1 (1972).
3. W. A. Phillips, *J. Low Temp. Phys.* **7**, 351 (1972).
4. A. Szabo, *Phys. Rev. Lett.* **25**, 924 (1970).
5. R. I. Personov, E. I. AfShits, L. A. Bykovskaya, *Opt. Commun.* **6**, 169 (1972).
6. B. M. Kharlamov, R. I. Personov, L. A. Bykovskaya, *ibid.* **12**, 191 (1974).
7. A. A. Gorokhovskii, R. K. Kaarli, L. A. Rebanc, *JETP Lett.* **20**, 216 (1974).
8. P. M. Selzer, D. L. Huber, D. S. Hamilton, W. M. Yen, M. J. Weber, *Phys. Rev. Lett.* **36**, 813 (1976).
9. S. K. Lyo and R. Orbach, *Phys. Rev. B* **22**, 4223 (1980).
10. J. M. Hayes, R. P. Stout, G. J. Small, *J. Chem. Phys.* **74**, 4266 (1981).

11. See J. M. Hayes, R. Jankowiak, G. J. Small, in *Topics in Current Physics, Persistent Spectral Hole Burning: Science and Applications*, W. E. Moerner, Ed. (Springer-Verlag, New York, 1987), chap. 5, and other chapters therein.
12. *Amorphous Solids—Low Temperature Properties*, W. A. Phillips, Ed. (Springer-Verlag, New York, 1981).
13. R. I. Personov, in *Spectroscopy and Excitation Dynamics of Condensed Molecular Systems*, vol. 4 of *Modern Problems in Condensed Matter Sciences*, V. M. Agranovich and R. M. Hochstrasser, Eds. (North-Holland, Amsterdam, 1983), chap. 10.
14. J. M. Hayes, B. L. Fearey, T. P. Carter, G. J. Small, *Int. Rev. Phys. Chem.* **5**, 175 (1986).
15. F. H. Stillinger and T. A. Weber, *Science* **225**, 983 (1984).
16. J. M. Hayes and G. J. Small, *Chem. Phys.* **27**, 151 (1978).
17. B. L. Fearey, T. P. Carter, G. J. Small, *ibid.* **101**, 279 (1986).
18. J. Friedrich, D. Haarer, R. Silbey, *Chem. Phys. Lett.* **95**, 11 (1983).
19. J. Friedrich, J. D. Swalen, D. Haarer, *J. Chem. Phys.* **73**, 705 (1980).
20. J. Jäckle, *Z. Phys.* **257**, 212 (1972).
21. W. Breinl, J. Friedrich, D. Haarer, *Chem. Phys. Lett.* **106**, 487 (1984).
22. R. Jankowiak, G. J. Small, K. B. Athreya, *J. Phys. Chem.* **90**, 3896 (1986).
23. R. Jankowiak, R. Richert, H. Bässler, *ibid.* **89**, 4569 (1985).
24. R. Jankowiak, L. Shu, M. J. Kenney, G. J. Small, *J. Lumin.* **36**, 293 (1987).
25. S. Völker, *ibid.*, p. 251.
26. R. M. Macfarlane and R. M. Shelby, *ibid.*, p. 179.
27. R. Jankowiak and G. J. Small, *Chem. Phys. Lett.* **128**, 377 (1986); *J. Phys. Chem.* **90**, 5612 (1986).
28. C. A. Walsh, M. Berg, L. R. Narasimhan, M. D. Fayer, *Chem. Phys. Lett.* **130**, 6 (1986); *J. Chem. Phys.* **86**, 77 (1987); L. M. Molenkamp and D. A. Wiersma, *ibid.*, **83**, 1 (1985).
29. S. K. Lyo, in *Electronic Excitations and Interactions Processes in Organic Molecular Aggregates*, vol. 49 of *Springer Series in Solid State Science*, P. Reinecker, H. Haken, H. C. Wolf, Eds. (Springer-Berlin, New York, 1983), p. 215.
30. R. Jankowiak, G. J. Small, B. Ries, *Chem. Phys.*, in press.
31. J. C. Lasjaunias, R. Maynard, M. Vandorpe, *J. Phys. (Paris) Colloq.* **39**, C6-973 (1978).
32. J. C. Lasjaunias, R. Maynard, D. Tholouze, *Solid State Commun.* **10**, 215 (1972).
33. L. Guttman and S. M. Rahman, *Phys. Rev. B* **33**, 1506 (1986).
34. U. Buchenau *et al.*, *ibid.* **34**, 5665 (1986).
35. H. Härdle, G. Weiss, S. Hunklinger, F. Baumann, *Z. Phys. B* **65**, 291 (1987).
36. B. L. Fearey, R. P. Stout, J. M. Hayes, G. J. Small, *J. Chem. Phys.* **78**, 7013 (1983).
37. M. J. Kenney, R. Jankowiak, G. J. Small, unpublished results.
38. M. D. Fayer, private communication.
39. J. Friedrich and D. Haarer, in *Optical Spectroscopy of Glasses*, I. Zschokke, Ed. (Reidel, Dordrecht, Netherlands, 1986), p. 149.
40. A. Gorokhovskii, V. Korrovits, V. Palm, M. Trummal, *Chem. Phys. Lett.* **125**, 355 (1986).
41. S. Hunklinger and A. K. Raychaudhuri, in *Progress in Low Temperature Physics*, D. F. Brewer, Ed. (North-Holland/Elsevier, Amsterdam, 1986), vol. 9, p. 265.
42. M. Meissner and K. Spitzmann, *Phys. Rev. Lett.* **46**, 265 (1981).
43. J. Friedrich and D. Haarer, *Angew. Chem. Int. Ed. Engl.* **23**, 113 (1984).
44. This article is made possible by support from the Division of Materials Research of NSF through grant DMR-8612270.

